Andreas J. Horbach and Manfred Staat*

Optical strain measurement for the modeling of surgical meshes and their porosity

https://doi.org/10.1515/cdbme-2018-0045

Abstract: The porosity of surgical meshes makes them flexible for large elastic deformation and establishes the healing conditions of good tissue ingrowth. The biomechanic modeling of orthotropic and compressible materials requires new materials models and simulstaneoaus fit of deformation in the load direction as well as trannsversely to to load. This nonlinear modeling can be achieved by an optical deformation measurement. At the same time the full field deformation measurement allows the dermination of the change of porosity with deformation. Also the socalled effective porosity, which has been defined to asses the tisssue interatcion with the mesh implants, can be determined from the global deformation of the surgical meshes.

Keywords: Porosity, Orthotropy, Surgical mesh, Digital image correlation

1 Introduction

The main motivation for this work was to develop a method to determine material parameters for compressible surgical meshes for a specific material model. Normally, such meshes are characterized for their biocompatibility [1],[2],[3] and their interactions with the surrounding tissue. One outcome of in vivo experiments is that the effective porosity is an important geometric criterion for the biocompatibilty of mesh implants [5] .

Additionally the deformation behavior of surgical meshes under load was observed in the present study and evaluated with optical full field strain measurement by digital image correlation. From this the nonlinear stress-stretch behavior and the change in porosity were derived. It could be shown that it is possible to derive the porosity change via image correlation without recourse to the hyperelastic constitutive law.

***Corresponding author: Manfred Staat,** Biomechanics Laboratory, Institute for Bioengineering, Heinrich-Mußmann-Str.1, Jülich, Germany, e-mail: staat@fh-aachen.de
Andreas J. Horbach, Biomechanics Laboratory, Institute for Bioengineering, Heinrich-Mußmann-Str.1, Jülich, Germany, e-mail: horbach@fh-aachen.de

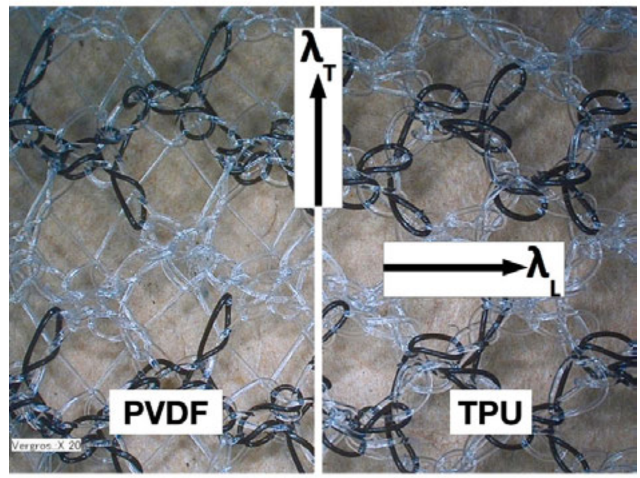

Fig. 1: Left side: PVDF-mesh; Right side: TPU - mesh

2 Material and Methods

2.1 Implants

Two different mesh types (FEG Textiltechnik mbH, Aachen, Germany) have been tested. The meshes have been produced with iron oxides to make them visible in MRI for test purposes and are not for clinical usage (but they have been used for research for hernia repair , see [3]). They are made out of PVDF (polyvinylidene difluoride) but one of them has a small amount of TPU (thermoplastic polyurethane) added to achieve softer properties. TPU and PVDF are no trading names but they are used to identify the meshes in presentation of results. The figure 1 shows the examined meshes with the principle stretching directions (L = longitudinal and T = transverse).

2.2 Optical Strain Measurement

With the aid of optical strain measurement, the deformation of materials can be measured during a tensile test. In this way, the anisotropic material behavior can be observed in a simple way. In the present case, a mesh sample was clamped into a tensile testing machine with a clamping distance of 50mm. The test started with a preconditioning of 2N for 3 cycles. Af-

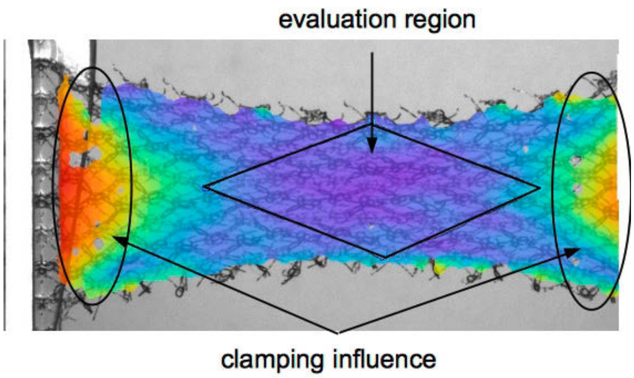

Fig. 2: Field of interest.

terwards the samples were extended individually at a speed of 30mm/min until failure. This test was performed for each mesh in transverse and longitudinal direction.

The mesh deformation is then measured with the digital image correlation software ISTRA 4D (Limess Messtechnik und Software GmbH, Krefeld or Dantec Dynamics GmbH, Ulm, Germany). A homogeneous measuring field is selected (compare to Fig2) to obtain the right Cauchy-Green deformation tensor **C**. Least squares fitting is performed with Matlab (The MathWorks, Natick, MA, USA) simultaneously for both mesh orientations with respect to uniaxial stress and biaxial stretch.

2.3 The Itskov Model

Soft tissues are incompressible like most other materials, which show large elastic deformations. Itskov and Aksel [6] have developed a material model which can also represent the large changes of area of knitted fabrics. The model has been modified and allied to sports wear in [7]. The strain energy function $W\left(\tilde{I}_r, \tilde{J}_r, I_3\right)$ is written with the generalized pseudo invariants $\tilde{I}_r, \tilde{J}_r$ of $\mathbf{C}$; I_3 is its determinant:

$$W\left(\tilde{I}_r, \tilde{J}_r, I_3\right) = \frac{1}{4}\sum_{r}^{N}\mu_r\left[\frac{1}{\alpha_r}\left(\tilde{I}_r^{\alpha_r}-1\right)+\frac{1}{\beta_r}\left(\tilde{J}_r^{\beta_r}-1\right)+\frac{1}{\gamma_r}\left(I_3^{-\gamma_r}-1\right)\right]$$

The material constants can be found by fitting with the property: $\mu_r > 0, \alpha_r \geq 0, \beta_r \geq 0$. A detailed calculation of the (true) Cauchy stress as derivative of W can be found in [8]

2.4 Effective Porosity

Mühl et al. (2008) [5] introduced the definition of the effective porosity for surgical meshes. They count only those pores as open, which are large enough for the ingrowth of the surrounding tissue. Mühl and Klinge use their concept of the effective porosity in different studies and compare the results with the physical definition of porosity [4],[3]. Effective porosity excludes all pores, which are smaller in diameter than a critical diameter which depends on the mesh material, but is typically 1 mm. They move a circle of critical diameter in each open pore and measure the effective pore area as the area which can be covered by the motion [5]. The effective porosity changes with deformation of pores during a deformation of the surgical mesh.

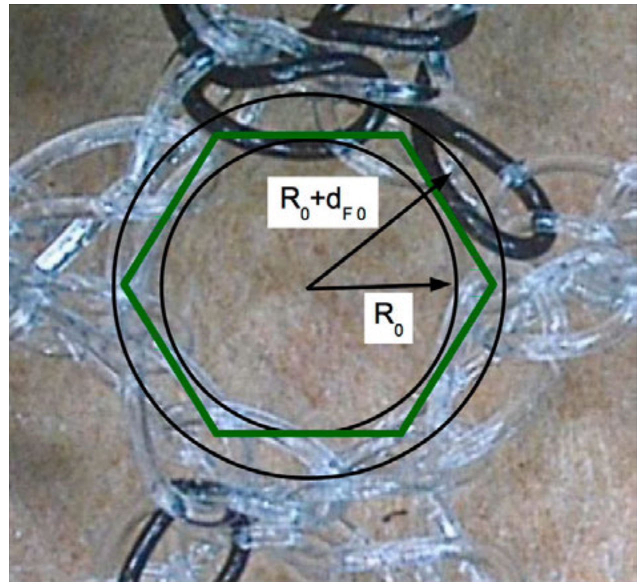

Fig. 3: Concept of determining the initial state of the two circles for effective porosity calculation.

To determine the effective porosity over the entire deformation, the pore size was measured using two representative pores under a digital microscope VHX-600 (Keyence, Japan). An inner circle with R_0 and an outer circle with $R_0 + d_{F,0}$ are measured in the undeformed mesh. The inner circle corresponds to the individual pore and the second circle corresponds to the pore with the surrounding mesh area (compare to figure 3). The ratio of the two surfaces can be used to determine the corresponding effective porosity for the respective area. We assume that the deformation is homogeneous over the entire evaluation range and calculate the deformation of the individual pore from a circle to an ellipse from the global optical strain measurement. Furthermore, the area of the mesh was assumed to be constant during the measurement. From these assumptions we were then able to calculate the porosity for each load step. This included the case that below a certain size of the minor axis of the ellipse, the pore is no longer considered effective and is therefore not counted in the effective area of porosity. The detailed calculation can be found in [8].

Tab. 1: Parameters for PVDF mesh

r	μ_r [MPa]	α_r	β_r	γ_r	$w_1^{(r)}$	$w_2^{(r)}$
1	0.19250	1.0	3.08488	0.0	1.0	0.0
2	0.3	3.89972	3.06319	0.0	0.70368	0.29632

Tab. 2: Parameters for TPU mesh

r	μ_r [MPa]	α_r	β_r	γ_r	$w_1^{(r)}$	$w_2^{(r)}$
1	0.22343	2.93787	1.0	0.0	0.0	1.0
2	0.05773	3.29183	4.86367	0.0	0.35339	0.64661

3 Results and Fittings

For the TPU and PVDF meshes a total number of 8 meshes each were tested. The following parameters were calculated: biaxial stretch in two directions, uniaxial Cauchy stress in load direction, and actual effective porosity during load steps.

3.1 Cauchy stress and Material Parameters

The tables 1 and 2 below show the results of the curve fit for the two meshes for N=2. For N>2 the computing time increased enormously, without any significant improvements of the results.

3.2 Effective Porosity

The figures Fig. 6 and 7 show the change of the effective porosity ϕ_{eff} in the evaluated region (according to the calculated porosity in Table 3) during deformation. Each figure shows two jump like drops of the porosity. These jumps represent the situation when one family of pores has a calculated diameter of $d < 0.6mm$, which means that these pores can be considered as fully closed. The critical loss of effective porosity occurs for the PVDF mesh at much lower stretch λ than for the TPU mesh.

3.3 Optical strain measurement with a higher resolution

Figure 8 shows results of the digital image correlation measurement of the TPU-mesh in a higher resolution of the strain field. It is visible that the strain is not as perfectly homoge-

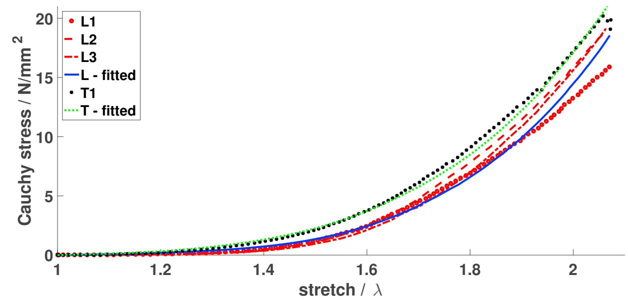

Fig. 4: Tensile tests in longitudinal (L) and transverse (T) direction and fits, PVDF - mesh

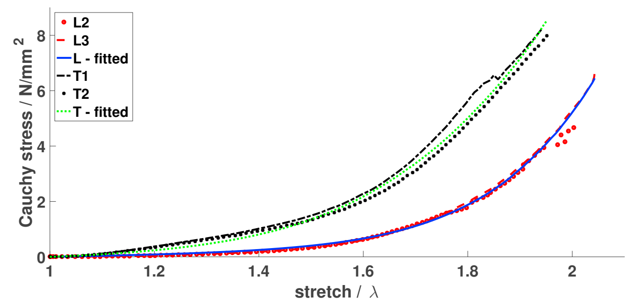

Fig. 5: Tensile tests in longitudinal (L) and transverse (T) direction and fits, TPU - mesh

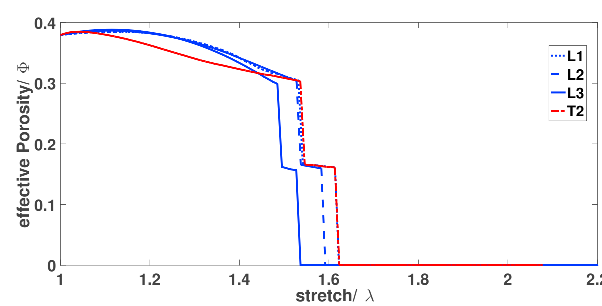

Fig. 6: Effective porosity under uniaxial loading as function of major principal stretch in loading direction, PVDF - mesh

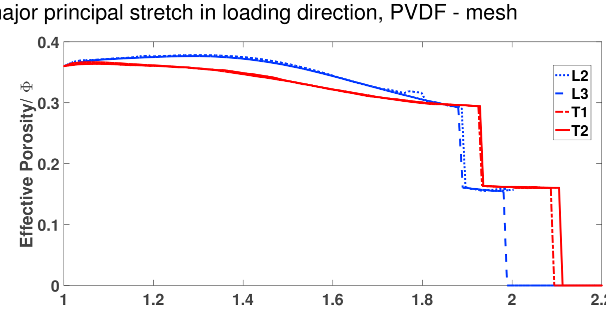

Fig. 7: Effective porosity under uniaxial loading as function of major principal stretch in loading direction, TPU - mesh

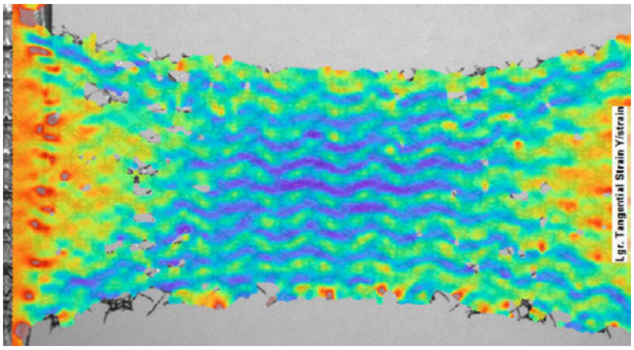

Fig. 8: Strain field with a higher resolution

neous as expected. Therefore, we plan to text an image based analysis of the local pore deformation.

4 Conclusion

The experiments have shown that optical strain measurement can be used to model compressible surgical meshes. Furthermore, the Itskov model could be successfully used simulate mechanical behavior of the tested surgical meshes. The effective porosity can be calculated from the observed global deformation of the implant.

However, due to its construction as a sum function, the Itskov model can quickly lead to very long computing times for curve fitting. This similarly effects the implementation of the Itskov model in programs for finite element analysis and numerical simulations. Therefore, a decision should be made after curve fit as to how large the respective N should be selected for the sum function in order to use the respective material parameters within an acceptable time.

Nevertheless, it has been shown that the change in effective porosity can be determined directly from global mesh deformation. For a preliminary assessment of the tolerability of the surgical meshes after implantation, the procedure described here can also be used completely without modeling.

Author Statement
Research funding: The authors state no funding involved. Conflict of interest: Authors state no conflict of interest. Informed consent: Informed consent is not applicable. Ethical approval: The conducted research is not related to either human or animals use.

References

[1] Darzi S, Urbankova I, Su K, White J, Lo C, Alexander D, et al. Tissue response to collagen containing polypropylene meshes in an ovine vaginal repair model. Acta Biomater. 2016;39:114–123.

[2] Coda A, Lamberti R, Martorana S. Classification of prosthetics used in hernia repair based on weight and biomaterial. Hernia 2012;16(1);9–20.

[3] Klosterhalfen B, Klinge U, Schumpelick V, Functional and morphological evaluation of different polypropylene-mesh modifications for abdominal wall repair. Biomaterials 1998;19(24):2235–2246.

[4] Klinge U, Klosterhalfen B, Birkenhauer V, Junge K, Conze J, Schumpelick V. Impact of polymer pore size on the interface scar formation in a rat model. J. Surg. Res. 2008;103(2):208–214.

[5] Mühl T, Binnebösel M, Klinge U, New objective measurement to characterize the porosity of textile implants. J. Biomed. Mater. Res. B: Appl. Biomater. 2008;84B(1):176–183.

[6] Itskov M, Aksel N, A class of orthotropic and transversely isotropic hyperelastic constitutive models based on a polyconvex strain energy function. Int. J. Solids Struct. 2004;41(14):3833–3848.

[7] Tanaka M, Noguchi H, Fujikawa, Sato M, Oi S, Kobayashi T, et al. Development of large strain shell elements for woven fabrics with application to clothing pressure distribution problem. CMES: Comput. Model. Eng. Sci. 2010;62(3):265–290.

[8] Horbach AJ, Duong MT, Staat M. Modelling of compressible and orthotropic surgical mesh implants based on optical deformation measurement. J Mech Behav Biomed Mater. 2017;74:400–410.

[9] Ciritsis A, Horbach AJ, Staat M, Kuhl CK, Kraemer N. Porosity and tissue integration of elastic mesh implants evaluated in vitro and in vivo. J Biomed Mater Res B Appl Biomater. 2018;106(2):827-833.